Differentiating Sonar Reflections from Corners and Planes by Employing an Intelligent Sensor

BILLUR BARSHAN, STUDENT MEMBER, IEEE, AND ROMAN KUC, SENIOR MEMBER, IEEE

Abstract—With conventional time-of-flight sonar ranging systems, it is impossible to differentiate a reflection from a plane and from a right-angle corner reflector. A multitransducer pulse/echo ranging system is described that differentiates these two reflectors by exploiting the physical properties of sound propagation. The amplitudes and ranges of reflected signals for the different transmitter and receiver pairs are processed to determine if the reflecting object is a plane or a right angle corner. In addition, the angle of inclination of the reflector with respect to the transducer orientation can be measured. Reflected signal amplitude and range values, as functions of inclination angle, provide the motivation for the differentiation algorithm. A system using two Polaroid transducers is described that correctly discriminates between corners and planes for inclination angles within ±10° of the transducer orientation. The two-transducer system is extended to a multitransducer array to allow the system to operate over an extended range. An analysis comparing processing effort versus estimation accuracy is performed. This approach is applied to the sonar map building problem. Sonar maps are generated in which planes and corners are distinguished by two different symbols that indicate their location and, for the plane, its orientation.

Index Terms—Acoustics, intelligent sensors, map building, robot navigation, sensors, signal processing, sonar, time-of-flight ranging.

I. INTRODUCTION

PREVIOUS attempts at producing sonar maps for vehicular robot navigation [1]–[3] have been only marginally successful because the methods for determining the location of reflecting objects were *ad hoc* and did not consider some of the pecularities of acoustic propagation. One such peculiarity is that the reflections from a plane and a right-angle corner are indistinguishable when a single transducer having a symmetric aperture is employed [4]. In this paper, we describe a multitransducer system to differentiate reflections from a plane and a right-angle corner and indicate its application for sonar map production.

We use the term *intelligent sensor* when the sensor signal processing algorithms interpret the observed data, the interpretation being based on the *physical principles* governing the sensor and a *model* of the environment that is being examined. In this case, we employ the model of the far-field behavior of a piston-type transducer having a circular aperture and the differences in the reflections from a plane and a corner are determined using geometrical wave propagation. This approach suggests a procedure to differentiate the two by implementing a multitransducer system that exploits the differences in the signal amplitudes and travel times.

In Section II, an overview of current sonar ranging systems is presented. Section III describes a physical model for transducer reflection process from planes and corners. In Section IV, a simple plane/corner differentiation algorithm is introduced. We then discuss the performance of the system employing a linear array of Polaroid transducers [5], which was implemented in our laboratory. Experimental and analytical results are compared in Section V and applications to sonar map building are described in Section VI.

II. CURRENT SONAR RANGING SYSTEMS

Most sonar ranging systems currently employ a single acoustic transducer that acts as both a transmitter and receiver [5], [6]. After the transmitted pulse encounters an object, an echo is detected by the same transducer acting as a receiver. An example of a typical echo is shown in Fig. 1. A conventional *time-of-flight* (TOF) system produces a range value when the echo amplitude waveform first exceeds a threshold level. This is shown to occur at time t_0 in Fig. 1. A range measurement R_0 is obtained from the roundtrip time-of-flight by the following formula:

$$R_0 = \frac{ct_0}{2} \tag{1}$$

where c is the speed of sound in air.[1] A sonar map is generated by placing a dot at the computed range along the transducer line-of-sight. The transducer is then rotated to a new angle, another pulse is transmitted and the process is repeated. An equivalent map is produced when instead of rotating the transducer, multiple transducers mounted in a ring are employed [1].

Examples of actual TOF dot patterns observed as a Polaroid transmitter/receiver (T/R) sweeps across a plane and a corner are shown in Fig. 2. Each dot was produced along the transducer line-of-sight as the transducer was rotated at angular increments of 0.9°. We note that with
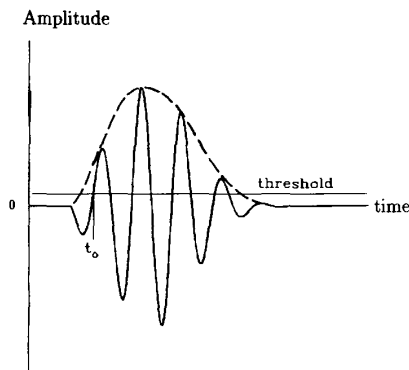
[1]$c = 343.5$ m/s at 20° [7].

Amplitude

Fig. 1. The typical echo observed in an ultrasound ranging system is indicated by the solid line. The waveform first exceeds the threshold at time t_0. Some systems determine the time-of-flight from the envelope of the echo, shown by the dashed line.
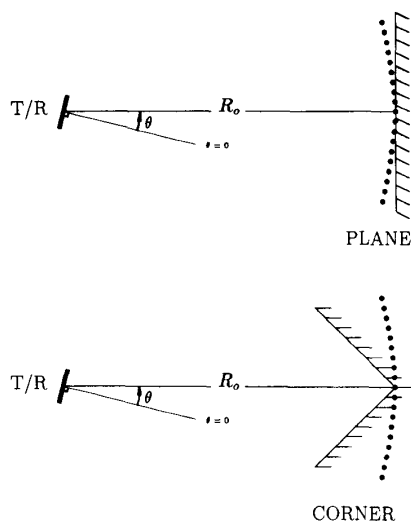

PLANE

CORNER

Fig. 2. TOF dot patterns of a single transducer produced by the plane and right-angle corner reflectors. The definition of the inclination angle θ for the plane and the corner is shown.

a single transducer, the dot patterns for the plane and corner are identical, illustrating the problem at hand. As shown later, the echo amplitude decreases as the transducer orientation deviates from normal incidence. This deviation is measured by the *inclination angle* θ as shown in Fig. 2. For the plane, θ indicates the angle from the transducer line-of-sight to the normal of the plane. For the corner, it is the angle to the line of intersecting planes that defines the corner.

When the magnitude of the inclination angle is greater than 10°, the echo amplitude falls below the threshold level, here equal to −30 dB relative to the amplitude at normal incidence, and no TOF dot is produced. It can be shown that the threshold level determines the effective angular beam width of the transducer [4]. Time-controlled gain amplifiers are commonly employed to compensate for the spreading loss due to diffraction and attenuation

[6], so that the reflection amplitude can be considered to be independent of range.

In addition to planes and corners, *edges* should also be included to complete the world model of the interesting spaces. An edge is a convex corner which is formed when two intersecting half-planes make an angle of 270°, whereas this angle is 90° for a concave corner. It has been shown that the reflection amplitudes from edges are typically much smaller than those from corners and planes, and exceed the threshold only when the distance between the transducer and the edge is small [8]. Hence, the reflections from edges will not be considered in this paper.

III. PHYSICAL MODELS

We present a physical model that describes the transducer reflection process from planes and corners. This model will demonstrate that the corner and the plane cannot be differentiated by using a single transducer that has a symmetric aperture, such as the circular aperture of the Polaroid sensor.

When the radius of the transmitting aperture a is much larger than the acoustic wavelength λ, the radiation forms a directed beam. This type of transmitter is commonly modeled by a flat piston of radius a, enclosed in an infinitely large baffle, that is vibrating at frequency f. The beam pattern that is produced has two distinct regions: the *near zone (Fresnel zone)* and the *far zone (Fraunhofer zone)* as shown in Fig. 3 [6].

In the near zone, the beam is contained within a cylinder of diameter $2a$, where a is the transducer radius. This zone extends from the face of the transmitter to a range approximately equal to a^2/λ. In the far zone of the single transducer, the beam diverges with *half-angle* θ_0 where

$$\theta_0 = \sin^{-1}\frac{0.61\lambda}{a}. \tag{2}$$

Note that θ_0 has frequency dependence.[2] For our system, $\lambda = 5.72$ mm and $a = 20$ mm. This corresponds to a near zone of 70 mm and a θ_0 of 10°.

In this paper, we are more interested in the far zone characteristics. In the far zone, the propagating pulse is considered to be a series of plane waves on the dimension scale of the receiving aperture. The signal is detected as these plane waves sweep across the aperture of the receiver. We will simplify the complicated equations that describe the transducer field [9] to provide analytic forms that are more intuitive, but yet provide useful results. From experiments, we find that the beam pattern for the pressure amplitude $p(\theta)$ of the transmitting transducer can be modeled by:

$$p(\theta) = p_{max} \exp\frac{-2\theta^2}{\theta_0^2} \tag{3}$$

[2] $\lambda = c/f$ and for the Polaroid transducer, $f = 60$ kHz is the nominal frequency. The spectrum of the pulse waveform is spread evenly about this value.
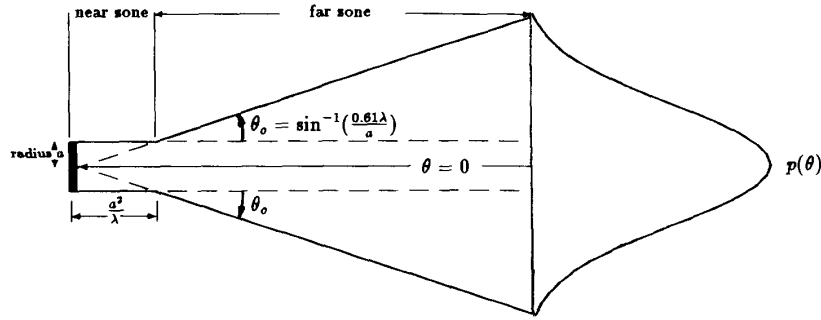
Fig. 3. The beam pattern for the piston model of the Polaroid transducer.

that is, a Gaussian form having standard deviation equal to $\theta_0/2$ shown in Fig. 3. This form is especially accurate for transmitted pulses that are time limited. For a pair of identical transducers, one acting as a transmitter, and the other as a receiver, the product of the two beam patterns is computed in order to determine the amplitude of the detected signal:

$$A(\theta_1, \theta_2) = A_{\max} \exp \frac{-2\theta_1^2}{\theta_0^2} \exp \frac{-2\theta_2^2}{\theta_0^2} \qquad (4)$$

where θ_1 and θ_2 are the inclination angles of the transmitter and reflector respectively, as shown in Fig. 4, and $A_{\max}$ is the amplitude that is observed when $\theta_1 = \theta_2 = 0$, i.e., the transducers are pointed at each other.

The model we propose for the environment considers the reflectors to be composed of smooth surfaces that act like mirrors. Such specular reflectors allow the transmitting/receiving (T/R) transducer to be viewed as a separate transmitter T, and a virtual receiver R' as illustrated in Fig. 5 [4]. Hence, in pulse-echo mode, the same transducer acts both as the transmitter and the receiver. By tracing rays exactly the same way as in mirror reflectors, we find that the inclination angle θ of the virtual receiver for the plane is opposite to that for the corner. For the reflection from a plane, and measuring angles in the counterclockwise directions, $\theta_1 = \theta$ whereas $\theta_2 = -\theta$, and for a corner, $\theta_1 = \theta_2 = \theta$. Substituting these values in (4) yields the same amplitude characteristics for both the plane and the corner:

$$A(\theta) = A_{\max} \exp \frac{-4\theta^2}{\theta_0^2}. \qquad (5)$$

Hence, the amplitude $A(\theta)$ decreases with increasing deviation θ from the transducer line-of-sight. Since we assume a time-variable gain amplifier is included, $A_{\max}$ is not a function of range R.

IV. PLANE/CORNER DIFFERENTIATION ALGORITHM

For symmetric transducer apertures, as indicated by (5), the detected signal $A(\theta)$ is an even function of the inclination angle θ, i.e., $A(\theta) = A(-\theta)$. Hence, planes and corners cannot be differentiated with a single transducer having a symmetric aperture, since they produce identical
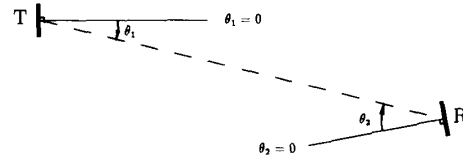
Fig. 4. A pair of identical transducers, one acting as a transmitter (T) and the other as a receiver (R). The dotted line indicates the path of the signal from the transmitter to the receiver.

PLANE

CORNER
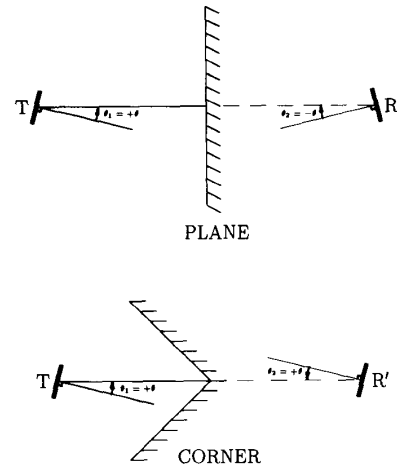
Fig. 5. For specular reflectors, a single transducer acting as the transmitter/receiver (T/R) can be viewed as a separate transmitter (T) and a virtual receiver (R').

reflections for a given *magnitude* of θ [4]. This was illustrated in Fig. 2.

To differentiate the corner from the plane, the difference in the sign of θ of the virtual receiver must be exploited. We propose to do this by replacing the single transducer of Fig. 5 by two transducers a and b, as shown in Figs. 6 and 7. Using this two-transducer configuration, amplitudes $A_{aa'}$, $A_{ab'}$, $A_{bb'}$, $A_{ba'}$ between the four T/R' pairs can be measured and exploited for the differentiation procedure as shown in Fig. 8. The corresponding ranges $R_{aa'}$, $R_{ab'}$, $R_{bb'}$, $R_{ba'}$ will be used for determining the inclination angle θ later.
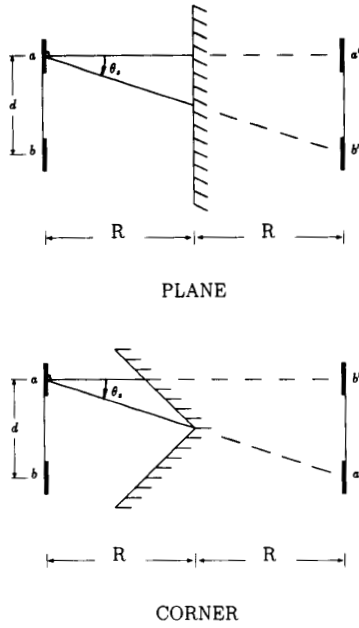
Fig. 6. Two-transducer system at zero inclination ($\theta = 0$) for plane and corner reflectors.
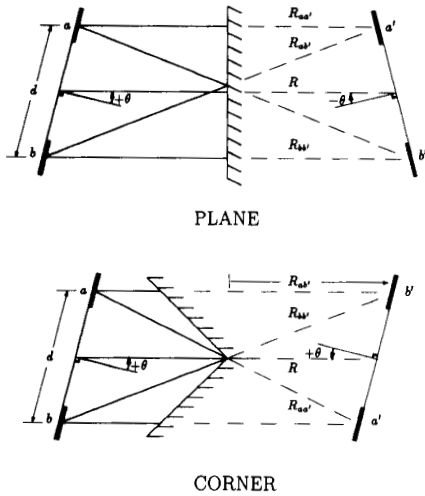

Fig. 7. Two transducer configuration. Geometry of θ, R, $R_{aa'}$, $R_{bb'}$, and $R_{ab'}$ for plane and corner reflectors are shown.

To understand the differentiation algorithm, it is helpful to express the amplitudes as functions of θ. The exact form of each amplitude curve is related to a complicated convolution of two Bessel functions. However, experimental curves of $A(\theta)$, given in [10], indicate that these curves can be accurately approximated by the following Gaussian forms:

For the plane,

$$A_{aa'}(\theta) = A_{bb'}(\theta) = A_{max} \exp \frac{-4\theta^2}{\theta_0^2} \qquad (6)$$
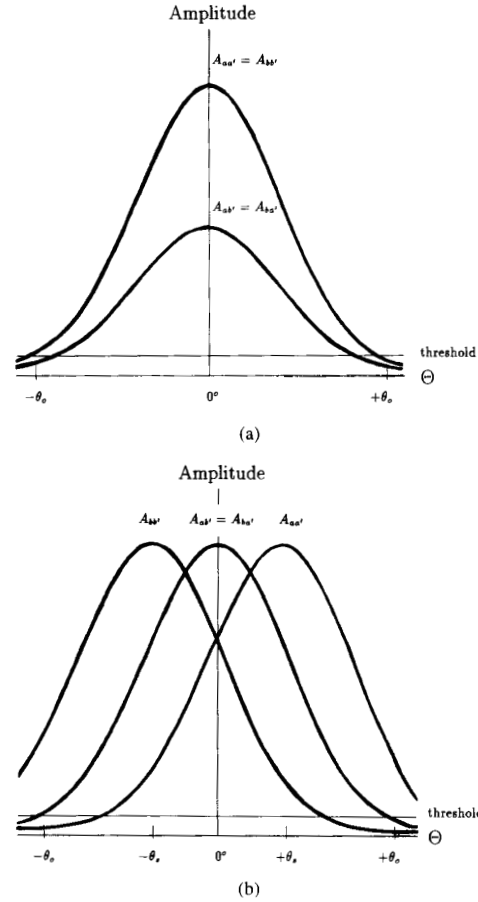

Fig. 8. (a) Amplitude versus θ curve for the plane reflector. (b) Amplitude versus θ curve for the corner reflector.

$$A_{ab'}(\theta) = A_{ba'}(\theta) = \underbrace{\left(A_{max} \exp \frac{-4\theta_s^2}{\theta_0^2} \right)}_{A'_{max}} \exp \frac{-4\theta^2}{\theta_0^2} \qquad (7)$$

where

$$\theta_s = \tan^{-1} \frac{d}{2R}. \qquad (8)$$

To illustrate these equations, consider a plane reflector at normal incidence ($\theta = 0$) as shown in Fig. 6. Then, transmitter a (or b) and virtual receiver a' (or b') directly point at each other and the corresponding signal $A_{aa'}$ (or $A_{bb'}$) takes its maximum value A_{max}. On the other hand, b' (a') lies at an angle θ_s with respect to a (b). This angle contributes a constant attenuation factor $\exp (-4\theta_s^2/\theta_0^2)$ to the amplitude of the signal $A_{ab'}$ ($A_{ba'}$). Due to this factor, its maximum amplitude, which occurs at $\theta = 0$, is $A'_{max} = A_{max} \exp (-4\theta_s^2/\theta_0^2)$. If θ deviates from $0°$, as shown in Fig. 7, the angles between the normals of each pair increase as 2θ. Hence, for a plane, $\theta = 0$ is the orientation when all four signals have their maximum amplitudes.

For the corner,

$$A_{aa'}(\theta) = A_{\max} \exp \frac{-4(\theta - \theta_s)^2}{\theta_0^2} \qquad (9)$$

$$A_{bb'}(\theta) = A_{\max} \exp \frac{-4(\theta + \theta_s)^2}{\theta_0^2} \qquad (10)$$

$$A_{ab'}(\theta) = A_{ba'}(\theta) = A_{\max} \exp \frac{-4\theta^2}{\theta_0^2}. \qquad (11)$$

Referring to Fig. 6, for a corner reflector at $\theta = 0$, transducers a (b) and b' (a') directly point at each other and the corresponding signal $A_{ab'}$ ($A_{ba'}$) takes its maximum value $A_{\max}$. The receiver a' (b') lies at an angle θ_s with respect to a (b) which attenuates the signal $A_{aa'}$ ($A_{bb'}$) at zero inclination. The maximum value of $A_{aa'}$ occurs at angle $\theta = +\theta_s$, when transmitter a is directly looking at virtual receiver a', hence $A_{aa'}(+\theta_s) = A_{\max}$. Similarly, the maximum value of $A_{bb'}$ occurs when $\theta = -\theta_s$.

For the plane, all amplitude curves [Fig. 8(a)] are symmetric around $\theta = 0$, where they take their maximum values. The maximum amplitude of the $A_{ab'}$ ($A_{ba'}$) curve, as given in (7), depends upon the $d/2R$ ratio given by (8). For the corner, all the signals [Fig. 8(b)] have the same $A_{\max}$ but the angles at which their maxima occur are determined by this ratio. However, $A_{ab'}$ ($A_{ba'}$) curve is always symmetric about $\theta = 0$. This difference between the plane and the corner characteristics is due to the configuration of virtual receivers, which was derived purely from the physics of reflection.

Let us consider what happens as θ_s is decreased by changing the values of d and/or R. For the plane, all curves remain symmetric about $\theta = 0$ but the magnitudes of $A_{ab'}(\theta)$ and $A_{ba'}(\theta)$ increase. In other words, there is more overlap between the beam patterns of the corresponding transducers. For the corner, $A_{aa'}(\theta)$ and $A_{bb'}(\theta)$ increasingly overlap with no change in magnitude. If θ_s is increased, opposite effects are observed. These results will be employed later for choosing a separation d for a given range R.

Due to noise effects, the actual amplitude measurement shows statistical variation which is modeled by additive random noise n:

$$A_{\text{meas}}(\theta) = A(\theta) + n. \qquad (12)$$

The noise can be described by a probability density function having zero-mean and variance σ^2. In our system, the sources of noise include:

1) *transducer bias voltage fluctuations* [5] which cause a variation of detected amplitude,

2) *thermal noise* in the electronics, and

3) *amplitude quantization error* due to sampling the signal with a finite number of bits.

Experiments were performed to estimate the total noise variance and it was observed that σ, the standard deviation of noise, is equal to 2% of $A_{\text{meas, max}}(\theta)$ and that σ is constant with range. Amplitude curves incorporating σ are redrawn in Fig. 9. In each case, the middle curve repre-
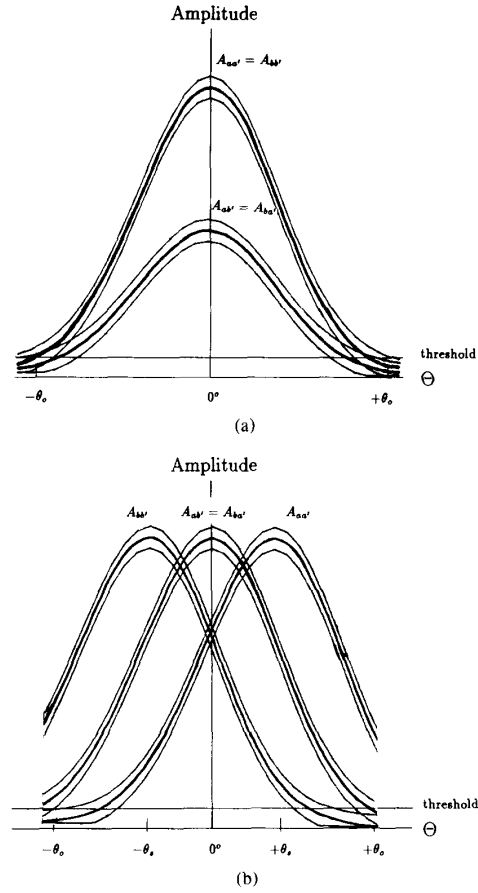

Fig. 9. (a) Curves incorporating the noise effects ($\pm 3\sigma$) for the plane reflector. (b) Curves incorporating the noise effects ($\pm 3\sigma$) for the corner reflector.

sents the mean value of the measured values $A_{\text{meas}}(\theta)$, whereas the upper and lower curves correspond to $\pm 3\sigma$ values, respectively. Assuming Gaussian statistics, amplitude measurements will be within $\pm 3\sigma$ of the mean value 99.7% of the time [11].

To identify the reflector, we compare the magnitudes of four amplitude curves. To provide statistical robustness, one amplitude measurement is taken to be *greater* than another only if the difference is greater than 6σ. Following this line of thought and referring to Fig. 9, the differentiation algorithm is:

decide PLANE if

$$A_{aa'}(\theta) - A_{ab'}(\theta) > 6\sigma \quad \text{AND}$$

$$A_{bb'}(\theta) - A_{ab'}(\theta) > 6\sigma \qquad (13)$$

decide CORNER if

$$A_{ab'}(\theta) - A_{aa'}(\theta) > 6\sigma \quad \text{OR}$$

$$A_{ab'}(\theta) - A_{bb'}(\theta) > 6\sigma. \qquad (14)$$

These conditions are mutually exclusive and when the relevant amplitudes differ by 6σ, it is always possible to make

a decision. When neither condition holds due to noise effects, which usually occurs for $|\theta| > 10^0 \approx \theta_0$, the object type is left indeterminate. To improve the ability to make decisions, the value of σ is used to choose the separation d between the two transducers, as shown later.

A. Inclination Angle Determination

To estimate the value of θ, we employ the four range measurements between the T/R' pairs. Using geometrical optics, analytic expressions for the range values $R_{aa'}$ and $R_{ab'}$ as a function of θ are determined, assuming the transducers are points located in the center of their apertures [10]. The true range, denoted by R, is the distance from the center of the transducer system to the object. Referring to Fig. 7 these functions for the plane are given by

$$R_{aa'\text{plane}} = R - \frac{d}{2}\sin\theta \tag{15}$$

$$R_{bb'\text{plane}} = R + \frac{d}{2}\sin\theta \tag{16}$$

$$R_{ab'\text{plane}} = R_{ba'\text{plane}} \cong \sqrt{R^2 + \frac{d^2}{4} - Rd\sin\theta} \tag{17}$$

where d is the distance between the centers of a and b. For the corner, the geometry of Fig. 7 gives

$$R_{aa'\text{corner}} = \sqrt{R^2 + \frac{d^2}{4} - Rd\sin\theta} \tag{18}$$

$$R_{bb'\text{corner}} = \sqrt{R^2 + \frac{d^2}{4} + Rd\sin\theta} \tag{19}$$

$$R_{ab'\text{corner}} = R_{ba'\text{corner}} = R. \tag{20}$$

These ranges are plotted in Fig. 10 where they are observed to be approximately linear functions of θ for $|\theta| \leq 10^0$.

We develop separate angle computation algorithms for the corner and the plane, that are applied after the differentiation has been made. To obtain reliable angle measurements, we must avoid the low amplitude signals that are typically corrupted by noise. From the geometry of the two-transducer system, shown in Fig. 7, expressions for the inclination angles of the plane θ_p and the corner θ_c are equal to

$$\theta_p = \sin^{-1}\frac{R_{bb'} - R_{aa'}}{d} \tag{21}$$

$$\theta_c = \begin{cases} \sin^{-1}\dfrac{(R_{bb'} - s) - R_{ab'}}{d} \\ \quad \text{if } R_{bb'} - s \geq R_{ab'} \\[4pt] \sin^{-1}\dfrac{(R_{aa'} - s) - R_{ab'}}{d} \\ \quad \text{if } R_{aa'} - s \geq R_{ab'} \end{cases} \tag{22}$$
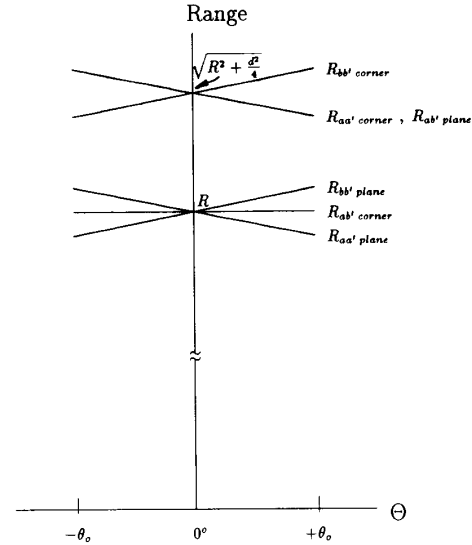

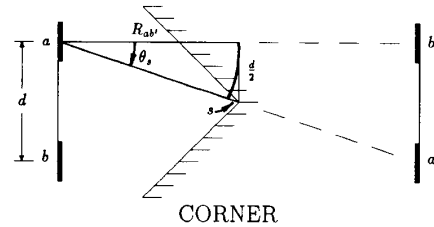Fig. 10. Range versus θ for small angles.

Fig. 11. Geometry of the correction term s for calculation of θ_c.

where s is a correction term, shown in Fig. 11, such that $\theta_c = 0$ for zero inclination:

$$s = \sqrt{R_{ab'}^2 + \frac{d^2}{4}} - R_{ab'}. \tag{23}$$

For the corner, the knowledge of θ allows us to place a *dot* on a sonar map, corresponding to the point of intersection of surfaces defining the corner, at the correct range and inclination angle. For a plane, a *line* is placed at the surface of the plane. Note that the inclination of the line in the sonar map corresponds to the true angle of the plane relative to the transducer system. For the corner, however, the angle of the surfaces defining the corner with respect to the transducer line-of-sight cannot be determined due to the physics of reflection. Only the angle to the line joining these two surfaces can be determined.

B. Limits on Separation Between Transducers

The ratio of transducer separation to reflector range (d/R), is important for making a correct differentiation since it is a measure of how well the amplitude characteristics of the plane and corner are separated. In the limit that this ratio goes to zero, the behavior of the two transducer system resembles that of a single transducer. In this

case, all the amplitude curves are identical and it is not possible to distinguish planes and corners.

For a given range R, we first find the lower and upper limits for transducer separation d. The noise variance σ, described above, determines d_{min}, the minimum transducer separation for plane/corner differentiation. Suppose that the two-transducer system with infinitesimal d is looking at a plane at normal incidence ($\theta = 0$). In this case, $A_{ab'}(\theta)$, $A_{ba'}(\theta)$ of (7) and $A_{aa'}(\theta)$ and $A_{bb'}(\theta)$ given by (6) are all equal. As d is increased, $A_{ab'}(\theta)$ and $A_{ba'}(\theta)$ decrease in magnitude, since there is less overlap between the beam patterns of the corresponding transducers. Statistically reliable differentiation occurs 99.7% of the time when the amplitude difference between $A_{aa'}(\theta)$ and $A_{ab'}(\theta)$ is greater than 6σ [11]. Let us now apply this argument for reliable differentiation by comparing the amplitudes at $\theta = 0$, since the signal-to-noise ratio is maximum at zero inclination.

If $d \geq d_{min}$:
For the plane,

$$A_{ab'}(0) + 3\sigma \leq A_{aa'}(0) - 3\sigma. \qquad (24)$$

For the corner,

$$A_{aa'}(0) + 3\sigma \leq A_{ab'}(0) - 3\sigma. \qquad (25)$$

Substituting for $A_{aa'}(0)$ and $A_{ab'}(0)$ from (6) and (7), both (24) and (25) yield the following result for d_{min}:

$$d_{min} = \frac{R \tan \theta_0}{2} \sqrt{-\ln\left(1 - \frac{6\sigma}{A_{max}}\right)}. \qquad (26)$$

To determine the upper limit d_{max}, we consider the *beam divergence* of sonar sensors as defined by (2). Employing the virtual receiver approach, as shown in Fig. 12, we see that d_{max} corresponds to the separation for which the virtual receiver lies on the edge of the beam pattern of the other transmitter. Simple geometry yields:

$$d_{max} = 2R \tan \theta_0. \qquad (27)$$

For $d > d_{max}$, there will be no signal between a and b'. For a given separation d such that $d_{min} < d < d_{max}$, a *working range* (R_{min}, R_{max}) can be defined for the two transducer system. For ranges $R_{min} < R < R_{max}$, a receiver detects the signals from *both* transmitters, a necessary condition for plane/corner differentiation and angle of inclination measurement. Employing equations (26) and (27), the limits of the working range are given by:

$$R_{min} = \frac{d}{2 \tan \theta_0} \qquad (28)$$

$$R_{max} = \frac{2d}{\tan \theta_0 \sqrt{-\ln\left(1 - \frac{6\sigma}{A_{max}}\right)}}. \qquad (29)$$

By increasing d, we can extend the maximum working range of the system to any desired value. However, this causes the minimum working range also to increase. To
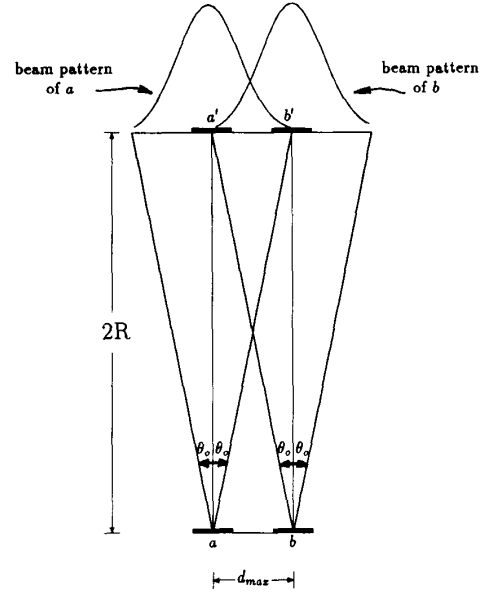

Fig. 12. Maximum d/R ratio as determined by beam divergence θ_0.

resolve this problem, multiple transducers in a *linear array* can be employed as described in the next section.

C. A Linear Array of Transducers

Let us consider the linear array configuration of transducers shown in Fig. 13. For a given range R, we want to choose the pair with the d/R ratio that allows us to make the most reliable differentiation between the plane and the corner. Applying the above argument, we choose the following average value for d:

$$d = \frac{d_{min} + d_{max}}{2}. \qquad (30)$$

Once the pair of the array elements having this approximation separation is selected, range and inclination angle calculations follow the same way as before.

To improve further the linear array system performance, it might seem reasonable to employ all the transducers in the array. Suppose that the array consists of N pairs of transducers as in Fig. 13. In this case, since there are $2N$ transducers, $4N^2$ amplitude, and $4N^2$ range measurements are available. However, considering only the N pairs symmetric around the middle of the array, the previous analysis extends directly and the processed data is of order $8N$. Let us consider estimating the inclination angle θ only, since range estimation will follow similarly.

Suppose that using information from only the ith pair, where $1 \leq i \leq N$, the estimate of θ is $\tilde{\theta}_i$. To incorporate data from all N pairs, we propose the following linear estimator:

$$\tilde{\theta} = \sum_{i=1}^{N} w_i \tilde{\theta}_i \qquad (31)$$
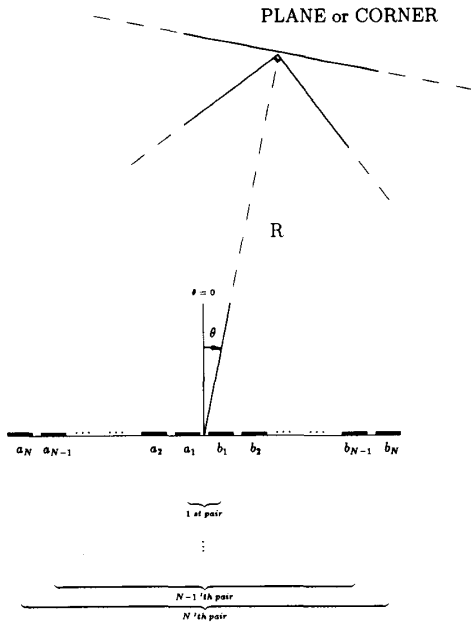
Fig. 13. A linear transducer array of $2N$ transducers.

where w_i are unknown weights to be determined with constraint

$$\sum_{i=1}^{N} w_i = 1. \qquad (32)$$

The constraint equation can be rewritten as:

$$g(w_1, \cdots, w_N) \triangleq \sum_{i=1}^{N} w_i - 1 = 0. \qquad (33)$$

The error ϵ is the difference between the estimated value $\tilde{\theta}$ and the true angle θ:

$$
\begin{aligned}
\epsilon &\triangleq \tilde{\theta} - \theta \\
&= \sum_{i=1}^{N} w_i \tilde{\theta}_i - \theta \\
&= \sum_{i=1}^{N} w_i \tilde{\theta}_i - \sum_{i=1}^{N} w_i \theta \\
&= \sum_{i=1}^{N} w_i \underbrace{(\tilde{\theta}_i - \theta)}_{\epsilon_i} \\
&= \sum_{i=1}^{N} w_i \epsilon_i.
\end{aligned}
\qquad (34)
$$

Since both positive and negative deviations are equally probable, ϵ is assumed to be a zero-mean random variable. In the following, it is also assumed that errors from different pairs are uncorrelated. Taking the expected

value, we get:

$$E\{\epsilon_i \epsilon_j\} = \delta_{ij} \sigma_i^2 \qquad (35)$$

where σ_i^2 is the variance of the error from the ith pair and δ_{ij} is the Kronecker delta. With these assumptions, the mean squared error is given by:

$$
\begin{aligned}
E\{\epsilon^2\} &= E\left\{ \left(\sum_{i=1}^{N} w_i \epsilon_i \right)^2 \right\} \\
&= \sum_{i=1}^{N} w_i^2 E\{\epsilon_i \epsilon_j\} \\
&= \sum_{i=1}^{N} w_i^2 \sigma_i^2.
\end{aligned}
\qquad (36)
$$

We now minimize the mean squared error with the constraint given by (33) on the weights. Employing the method of Lagrange multipliers [13], the function to be minimized becomes:

$$
\begin{aligned}
f(w_1, \cdots, w_N, \lambda) &= E\{\epsilon^2\} + \lambda g(w_1, \cdots, w_N) \\
&= \sum_{i=1}^{N} w_i^2 \sigma_i^2 + \lambda \left(\sum_{i=1}^{N} w_i - 1 \right)
\end{aligned}
$$
$$(37)$$

with λ being the Lagrange multiplier. Taking partial derivatives with respect to w_i and λ leads to $N + 1$ equations in $N + 1$ unknowns:

$$\frac{\partial f}{\partial w_i} = 2 w_i \sigma_i^2 + \lambda = 0 \qquad 1 \le i \le N \qquad (38)$$

$$\frac{\partial f}{\partial \lambda} = \sum_{i=1}^{N} w_i - 1 = 0 \qquad (39)$$

where (39) is the constraint equation as before. The solution to the resulting system of equations is:

$$\lambda = \frac{-2}{\sum_{k=1}^{N} (1/\sigma_k^2)} \qquad (40)$$

and the set of weights

$$w_i^* = \frac{\frac{1}{\sigma_i^2}}{\sum_{k=1}^{N} (1/\sigma_k^2)} \qquad 1 \le i \le N. \qquad (41)$$

Hence, given the noise variance for each of N pairs, we can make a better estimate employing the optimal weights w_i^*. In the next section, we provide experimental results to verify this analysis.

V. Experimental Results

The two-transducer system of Fig. 7 was implemented using two Polaroid sensors separated by $d = 80$ mm. This

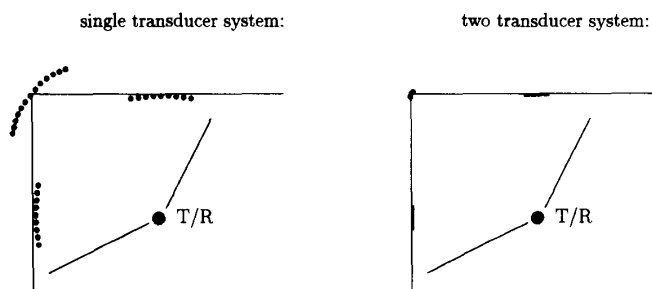single transducer system: two transducer system:

Fig. 14. Comparison of sonar maps for single and two transducer systems. In the two transducer system, it is possible to distinguish planes from corners by two different symbols.

system was mounted on a stepper motor producing angular increments of 0.9°. Experiments were run for corner and plane reflectors placed at ranges 200 mm $\leq R \leq$ 1600 mm from the transducer system. For a given range value, both a plane and a corner were scanned taking 100 measurements at each step of the motor. From this information, the mean value and the standard deviation σ of each amplitude measurement were calculated. These results indicated that σ was constant with range.

Experiments using a linear array of six densely packed Polaroid transducers verified the analysis for the linear array. At $R = 300$ mm, when information from each of three pairs is merged, the standard deviation of the inclination angle estimate was observed to be equal to 1.68°. Selecting the transducer pair spaced according to (30) produced a standard deviation value equal to 1.85°, which is greater by 10%. The modest improvement achieved by employing the three pairs in the array, however, is obtained at a cost of increasing the processing time threefold compared to using only a single pair.

Our multitransducer system has several limitations. In some cases, a decision cannot be made due to the small amplitude of some reflections. This usually occurs for $|\theta| \geq 10°$, for which the signal-to-noise ratio is low. In these cases, the object type is left indeterminate. Also, the reflecting corner or plane must have a dimension larger than the extent of the array to allow all transmitter and receiver pairs to communicate. This may limit the extent of the array for applications in a cluttered environment.

VI. APPLICATIONS TO SONAR MAP BUILDING

The advantages of the multitransducer array over the conventional single transducer system for sonar map building is shown in Fig. 14. A two transducer sensor system is situated to generate a sector scan of a corner and two planes. As shown above, the single transducer system produces identical dot patterns for corners and planes. The multitransducer system can generate a small line for a plane, showing both its distance from the transducers and its orientation. For the corner reflector, a dot is generated at the intersection point of the two planes that define it. This is because a multitransducer system can determine θ and put the dot in the direction, whereas a single-transducer system can only generate dots along its line of sight. The effects of noise cause slight errors in the dot and line locations.

VII. SUMMARY

We have described a multitransducer system in a simple, uncluttered environment consisting of specularly reflecting planes and corners. This "bottom-up" type of approach is useful for understanding the behavior of the system. As we complicate the system and the environment step-by-step, we accumulate more insight about the problem and its solutions. Algorithms for differentiating a plane from a right-angle corner reflector have been described. For the two-transducer system, the amplitudes and ranges for the four transmitter and receiver pairs provide sufficient information to determine if the reflecting object is a plane or a right-angle corner, as well as the inclination angle θ. It is possible to improve the results by using information from an array of sensors. To recognize corners and planes, the dimensions of the plane or corner reflector must be greater than the extent of the multitransducer system. Otherwise, the paths for the echos may not exist.

Experimentally observed amplitude and range data provided the motivation for the algorithms that are employed in the computations. Correct discrimination was made for inclination angles within $\pm 10°$ of normal incidence which is approximately equal to the beam width of the transducer. The limitations of the technique were described. The improvement in generating a sonar map with our multitransducer system was illustrated.

REFERENCES

[1] H. P. Moravec and A. Elfes, "High resolution maps from wide angle sonar," in *Proc. IEEE Int. Conf. Robotics and Automation*, 1986, pp. 116–121.

[2] J. L. Crowley, "Dynamic world modeling for an intelligent mobile robot using rotating ultrasonic ranging device," in *Proc. IEEE Int. Conf. Robotics and Automation*, 1985, pp. 128–135.

[3] S. Tachi and K. Komoriya, "Guide dog robot," in *Proc. Second Int. Symp. Robotics*, Kyoto, Japan, 1984.

[4] R. Kuc and M. W. Siegel, "Physically-based simulation model for acoustic sensor robot navigation," *IEEE Trans. Pattern Anal. Machine Intell.*, vol. PAMI-9, no. 6, pp. 766–778, Nov. 1987.

[5] *Ultrasonic Range Finders*, Polaroid Corp., 1982.

[6] P. N. T. Wells, *Biomedical Ultrasonics*. New York: Academic, 1977.

[7] R. C. Weast, *CRC Handbook of Chemistry and Physics*, 54th ed. Cleveland, OH: Chemical Rubber Co., 1973, p. E49.

[8] R. Kuc and B. Barshan, "Navigating vehicles through an unstructured environment with sonar," in *Proc. IEEE Int. Conf. Robotics and Automation*, 1989, pp. 1422–1426.

[9] P. M. Morse and K. U. Ingard, *Theoretical Acoustics*. New York: McGraw-Hill, 1968.

[10] R. Kuc and Y. D. Di, "Intelligent sensor approach to differentiating sonar reflections from corners and planes," in *Proc. Int. Congr. Intelligent Autonomous Systems*, Amsterdam, The Netherlands, 1986.

[11] M. Schwartz and L. Shaw, *Signal Processing*. New York: McGraw-Hill, 1975.

[12] A. Elfes and L. Matthies, "Sensor integration for robot navigation: Combining sonar and stereo range data in a grid-based representation," in *Proc. IEEE Conf. Decision and Control*, 1987.

[13] L. W. Johnson, and R. D. Riess, *Numerical Analysis*. Reading, MA: Addison-Wesley, 1982, pp. 518–523.

[14] D. J. Kriegman, E. Triendl, and T. Binford, "A mobile robot: Sensing, planning and locomotion," in *Proc. IEEE Int. Conf. Robotics and Automation*, 1987, pp. 402–408.

[15] K. L. Boyer and A. C. Kak, "Color-encoded structured light for rapid active ranging," *IEEE Trans. Pattern Anal. Machine Intell.*, vol. PAMI-9, no. 1, pp. 14–28, Jan. 1987.

Billur Barshan (S'89) was born in Istanbul, Turkey, in 1964. She received the B.Sc. degrees in electrical engineering and in physics from Boğaziçi University, Istanbul, Turkey, in 1986, and the M.S.E.E. degree from Yale University, New Haven, CT, in 1988, where she is currently working toward the Ph.D. degree in electrical engineering.

She is a Research Assistant in the Intelligent Sensors Laboratory and her current research interests include applications of digital signal processing in characterizing motion with ultrasound and the limits of ultrasound sensors.

Roman Kuc (M'77–SM'89) received the B.S.E.E. degree from the Illinois Institute of Technology, Chicago, and the Ph.D. degree in electrical engineering from Columbia University, New York, NY.

From 1968 to 1975 he was a member of Technical Staff at Bell Telephone Laboratories, engaged in the design of audio recording instrumentation and in developing efficient digital speech coding techniques. From 1977 to 1979 he was a postdoctoral research associate in the Department of Electrical Engineering, Columbia University, and the Radiology Department of St. Luke's Hospital, where he employed statistical estimation techniques to extract diagnostic information from reflected ultrasound signals. In 1979, he joined the Department of Electrical Engineering at Yale University, New Haven, CT, where he is pursuing problems in ultrasonic tissue characterization, biomagnetism, and intelligent sensors for robot applications. He is currently Director of Undergraduate Studies in Electrical Engineering. He is the author of *Introduction to Digital Signal Processing* (New York: McGraw-Hill).

Dr. Kuc is the IEEE Acoustics, Speech, and Signal Processing Society representative on the Steering Committee of the IEEE TRANSACTIONS ON MEDICAL IMAGING, an Associate Editor of *Ultrasonic Imaging*, and a member of the Shevchenko Scientific Society.